Advanced electron microscopy characterisation of important precipitation and ordering phenomena in shape memory systems

Reference:
Schryvers Dominique.- Advanced electron microscopy characterisation of important precipitation and ordering phenomena in shape memory systems
Shape memory and superelasticity - ISSN 2199-384X - 1:1(2015), p. 78-84
DOI: http://dx.doi.org/doi:10.1007/s40830-015-0006-3

Advanced electron microscopy characterisation of important precipitation and ordering phenomena in shape memory systems

Dominique Schryvers

EMAT, University of Antwerp, Groenenborgerlaan 171, B-2020 Antwerp, Belgium

Keywords: precipitation, ordering, TEM, SEM, Ni-Al, Ni-Ti

Abstract

The present paper discusses some important aspects of precipitation and ordering in alloy systems that show a martensitic transformation and can or are used as shape memory or superelastic metallic systems. The precipitates are investigated by a variety of conventional and advanced electron microscopy techniques, including atomic resolution, 3D slice-and-view, energy loss spectroscopy etc. Depending on the system, such secondary phases can decrease the probability of a displacive transformation by changing the phase stability in the system, such as in the case of Ni-Al or Ni-Ti-Pd, or can mechanically hinder the passage of the transformation interface, as in Ni-Ti-Nb. On the other hand, properly controlling the nucleation and growth of some precipitates can strongly improve the properties of some types of materials, as is the case for the well-known Ni_4Ti_3 precipitates.

Introduction

The appearance of shape memory (SM) and superelasticity (SE) behaviour in selected alloys is based on the diffusionless and reversible martensitic phase transformation. According to the classification scheme first presented by Cohen et al. (1979), this type of transformation implies a homogeneous lattice-distortive strain (as apposed to shuffle movements), which transforms one Bravais lattice into another one. Moreover, the strain needs to be shear dominated (as opposed to dominated by dilatations) so that an undistorted line exists between the parent and product phase. For a genuine martensitic transformation the kinetics and morphology also need to be dominated by the strain energy (as opposed to being due to atom vibrational displacements). Typical examples of alloys accommodating this type of transformation are low-carbon steel, some Cu-based alloys and Ni-Ti-based systems (although many other systems exist as well). However, for alloys to perform properly in the functional circumstances of shape memory and superelasticity as required by the conditions of a particular application, the system needs to be trained under well-defined thermal and mechanical conditions. As a result of this training (and especially its thermal component), the micro- and sometimes also the nanostructure of the alloy can become very complex, often including the precipitation of (meta)stable secondary phases in the form of precipitates, ordered structures, etc. Without these particular structural features the requested shape memory and superelastic behaviour would often not occur (or at least not to the satisfaction of the user), but since they are also often more stable than the metastable martensite phase, they can overrule the displacive martensitic transformation so the competition and interactions between the different structures needs to be understood very well.

In the present paper the focus will be on the use of advanced scanning and transmission electron microscopy (S/TEM) techniques used for the characterisation of such micro- and nanostructures. For a first example we return to conventional high resolution TEM (HRTEM) and to the Ni-Al system, an alloy that was heavily investigated in the second half of the previous century to understand the physical properties and driving forces of the (pre-)martensitic transformation. In the second example various more advanced S/TEM examples aiming for better quantification of the all-important but metastable Ni_4Ti_3 precipitates in near-equiatomic Ni-Ti will be discussed. For some last examples, we focus on precipitates occurring in ternary Ni-Ti-based systems, such as Ni-Ti-Pd and Ni-Ti-Nb. For technical details on the sample preparation and used microscopy techniques, we refer to the respective papers.

Results and discussion

Ni_5Al_3 in Ni-Al

For a long time the Ni-rich part of the Ni-Al system, i.e., between 62 and 66 at.% Ni, was considered as a potential candidate for high temperature SM behaviour since the transformation temperatures, although strongly depending on concentration, can go up to several hundreds of centigrades (Shapiro 1991). However, as is clear from the phase diagram originally published by Bradley & Taylor (Bradley

1937) and later refined by several others (see, e.g., Okamoto 2004), when treating or operating the material at elevated temperatures up to 700°C the stable Ni_5Al_3 structure nucleates in the austenite B2 matrix and this new structure does not transform to martensite so no SM behaviour exists anymore. In fact, the basic lattice of this orthorhombic **Ni_5Al_3** structure strongly resembles that of the tetragonal $L1_0$ martensite, the main difference being the accompanying diffusional component yielding a unit cell 4 times as large by doubling the shortest and one of the longest axes of the martensite cell and yielding twice as many variants (Schryvers 1995; Schryvers 1995a). As a result, the nucleation of this structure is also accompanied by the formation of so-called self-accommodating structures in which the internal strain is minimized by the combination of several variants. In Figure 1 an example of such a configuration is shown as observed at low magnification HRTEM in a $Ni_{62.5}Al_{27.5}$ sample annealed for 2h at 550°C and in which all three possible deformation variants are combined in 2 by 2 wings extending from a central nucleation point (Schryvers 1995). Despite the highly symmetric shape combining different variants and seen when observing the surrounding matrix along a $<111>_{B2}$ direction, the accommodation is not perfect and the matrix-precipitate interfaces contain equidistant interfacial dislocations to accommodate the remaining interfacial lattice mismatch between the two structures. Assuming the Ni_5Al_3 structure has its expected stoichiometric concentration, which equals the nominal composition of the $Ni_{62.5}Al_{27.5}$ alloy, the nucleation and growth of these precipitates is only accompanied with local short range atom diffusion and will not influence the concentration of the surrounding matrix. As a result also the (low) transformation temperature and martensite 14M fine structure will be the same as for the original material (Schryvers 1993). Furthermore, according to the phase diagram, when continuing the annealing for longer times, the entire B2 austenite matrix will transform into this stable twinned Ni_5Al_3 structure and no martensitic transformation can be observed anymore. When annealing quenched material with slightly higher Ni concentrations, e.g. $Ni_{65}Al_{35}$, which is in the martensite state even at these elevated temperatures (e.g., 550°C), the martensite lattice reorders directly into the Ni_5Al_3 structure, again stopping the possibility for any further displacive transformations (Schryvers 1995b). In this particular system, the nucleation and growth of the ordered Ni_5Al_3 structure thus strongly hinders potential applications as SM or SE system, certainly at elevated temperatures.

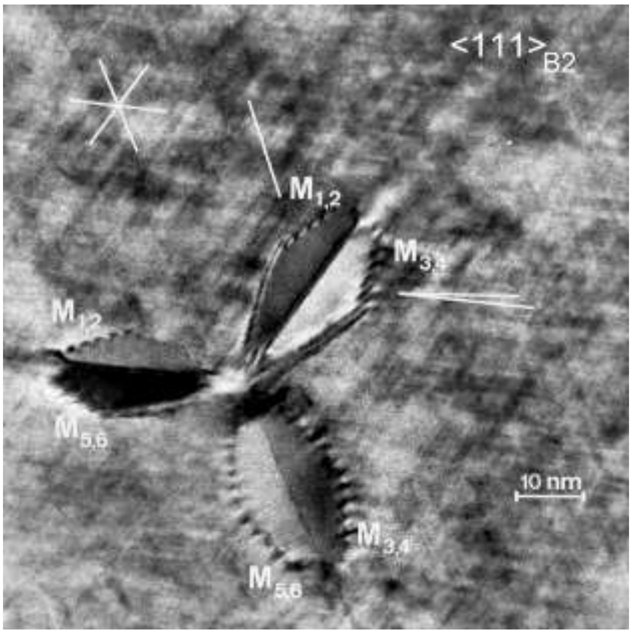

Figure 1: $<111>_{B2}$ low magnification HRTEM image of a star shaped Ni_5Al_3 precipitate in annealed $Ni_{62.5}Al_{27.5}$ and combining different variants to minimize deformation strains. Still, interface dislocations are seen between the precipitate and matrix. (the indices refer to the two possibilities of ordering for each deformation variant) (Schryvers 1995)

Ni_4Ti_3 in Ni-Ti

In contrast to the disturbing effects of the nucleation and growth of the Ni_5Al_3 structure in Ni-Al, the Ni_4Ti_3 precipitates nucleating in near-equiatomic Ni-rich Ni-Ti material are very important for the martensitic transformation and related SM and SE effects (Otsuka 2005). Although these precipitates are metastable and will thus disappear after prolonged annealing times, controlled thermo-mechanical treatments can create particular configurations of lenticular Ni_4Ti_3 precipitates in which the latter can act as nucleation sites of the transformation and support the SM behaviour at the microscopic level (Bataillard 1998). Moreover, due to the difference in concentration between the precipitates and the matrix and the resulting decrease of Ni in the latter upon precipitation, the annealing will stabilize the matrix concentration and thus the transformation temperatures, which are also in this system strongly dependent on composition (Frenzel 2010; Otsuka 2005; Tang 1997).

Using the multi slice least squares (**MSLS**) method we first determined the exact atomic structure of well-developed Ni_4Ti_3 precipitates in a $Ni_{52}Ti_{48}$ alloy solution treated at 950°C for 30min followed by water quenching and aging for 4h at 520°C (Tirry 2006). In this method, electron diffraction intensities measured by a calibrated CCD are compared with simulated dynamical intensities calculated using the multi slice method (Jansen 1998; Jansen 2002). By optimizing the match between the experimental and calculated intensities, including the thickness and small misalignments as unknown parameters, site occupations and small atom shifts can be determined. As a result the atomic positions of the Ni_4Ti_3 unit cell are refined, as shown in Figure 2a, with no change in the R-3 symmetry of the earlier proposed unit cell (Tirry 2006). The new unit cell also provides a better match between simulated and experimental high-resolution images, as seen in Figure 2b. The observed atom shifts are found to be compatible with the lattice deformation by which the $<111>_{B2}$ direction is compressed and the lens shaped precipitates are formed on $\{111\}_{B2}$ planes.

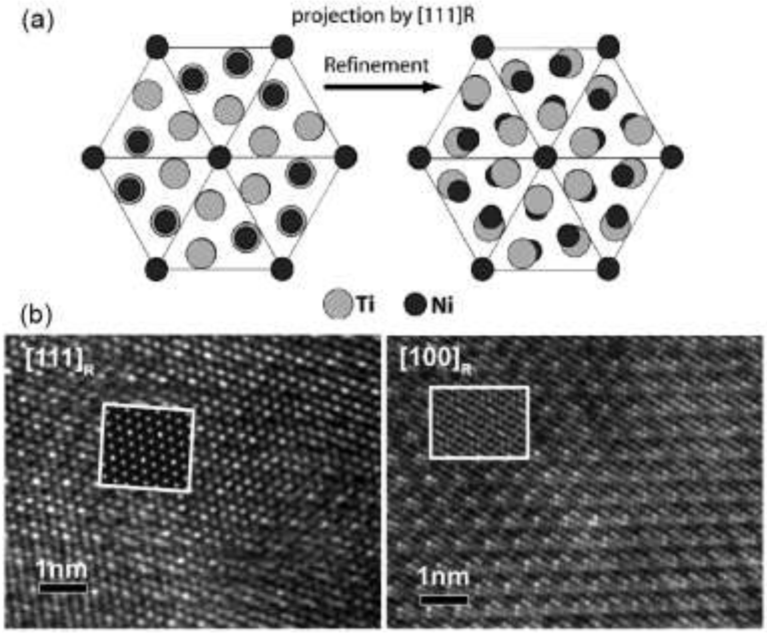

Figure 2: (a) Ni_4Ti_3 unit cell as determined using MSLS optimization and showing the atom shift when compared with the earlier model. (b) HRTEM images along two different zones including matching simulated insets. (the zones are defined in the rhombohedral (R) unit cell of the Ni_4Ti_3 structure) (Tirry 2006)

As a result of the collapse of one set of $\{111\}_{B2}$ planes upon formation of the Ni_4Ti_3 precipitates a **strain field** develops surrounding the precipitate. Since the martensitic transformation upon cooling can nucleate at these precipitates, often in the form of the intermediate R-phase (Bataillard 1998; Michutta 2006) this strain field is of vital importance for the SM and SE behaviour. From single conventional high resolution TEM (HRTEM) images of small precipitates produced in a $Ni_{51}Ti_{49}$ alloy subjected to a heat treatment of 1h at 950°C followed by water quenching and subsequently aged for 4h at 450°C the strain gradient in the surrounding matrix could be measured in 2D (Tirry 2005), while by combining two conventional HRTEM images obtained from different B2 zone axes, a 3D deformation matrix could be determined (Tirry 2009). The symmetry and parameters of the latter correspond well with the transformation matrix of the R-phase, suggesting that this strain field indeed supports the R-phase nucleation at the precipitate-matrix interface. An example of a 2D strain map surrounding two nearby nano-precipitates and obtained by Geometric Phase Analysis (GPA) (Hÿtch 1998) from a HRTEM image is shown in Figure 3a. At the same time, due to Ni-enrichment in the precipitate, the surrounding matrix is depleted in Ni. This could be shown by spot-probe energy dispersive X-ray analysis (EDX) and electron energy loss spectroscopy (EELS) measurements, again in solution treated

$Ni_{51}Ti_{49}$ but now annealed for 4h at 500°C, which revealed a small Ni-depleted region next to the precipitate and of approximately the same dimension as the latter (Yang 2005) (Figure 3b). Lowering the Ni content can also trigger the martensitic transformation, but recent results attribute a stronger effect to the strain field (Wang 2015).

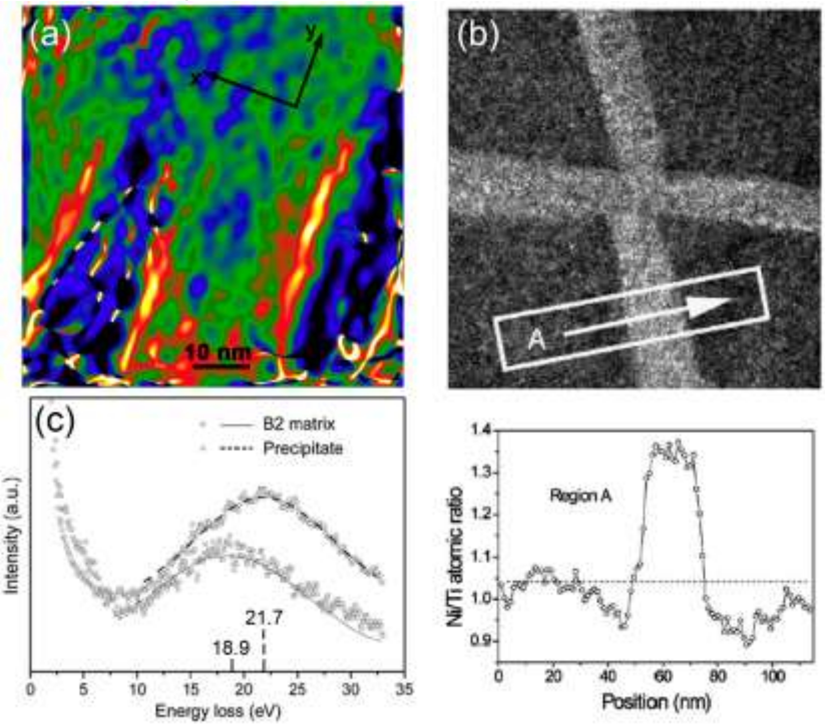

Figure 3: (a) GPA map showing the strain gradients next to the long edges of Ni_4Ti_3 nano-precipitates: the matrix is taken as a reference (green), the precipitates show a 1 to 2 % compression (blue) while the strongest relaxation (1 to 3%) occurs alongside the long edges of the precipitates (red to yellow). (b) EDX Ni-map of two crossing precipitates with an averaged trace revealing Ni-depletion next to the precipitate. (c) EELS plasmon of the precipitate and austenite matrix. (Yang 2005; Yang 2008)

EELS was also used on the same sample to determine the elastic moduli of the metastable Ni_4Ti_3 precipitates, by measuring the plasmon energy and comparing this with the value for the matrix as reference as shown in Figure 3c (Yang 2008). As a result it was concluded that the precipitates have a Young's modulus of 163±4 GPa, about 38% higher than that of the matrix, in other words the precipitates are harder than the matrix explaining why they are not deformed during the martensitic transformation of the austenite.

Although these intrinsic properties of a single Ni_4Ti_3 precipitate embedded in austenite B2 matrix are very relevant for understanding the transformation behaviour at the atomic scale, the macroscopic SM and SE behaviour will be more affected by the actual overall configuration and organisation of the Ni_4Ti_3 precipitates. For example, in polycrystalline samples the heterogeneity of the nucleation and growth of Ni_4Ti_3 precipitates has been found to yielding various kinds of multi-step transformations due to the existence of different areas of precipitates with various sizes and density (Khalil-Allafi 2002; Khalil-Allafi 2002a; Dlouhy 2003; Nishida 2003). Close to the grain boundary of grains of several micron in diameter many small precipitates exist, while the interior of the grains exhibit none or fewer but larger precipitates, resulting in different transformation paths and Ms temperatures in those different regions. In order to quantify these microstructures in three dimensions, **3D slice-and-view** was performed in a FIB/SEM yielding clear numerical differences between the various regions. In Figure 4a the 3D configuration of the 4 families of micron-sized Ni_4Ti_3 precipitates observed in the centre of a large grain in a $Ni_{50.8}Ti_{49.2}$ alloy solution treated at 1000°C for 1h, water quenched and annealed for 1h at 550°C, is shown, while Figure 4b shows the gradient from this region (right side) when moving closer to the grain boundary area (left side) with more but smaller precipitates (Cao 2011; Cao 2012).

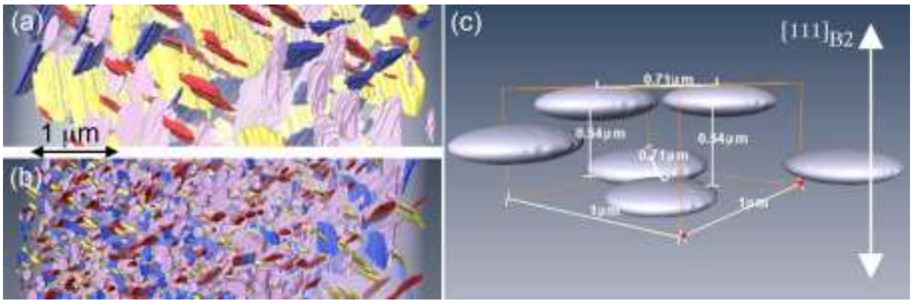

Figure 4: 3D configuration of Ni_4Ti_3 precipitates obtained by FIB/SEM slice-and-view in (a) the centre of a large grain and (b) closer towards the grain boundary (left). (c) The stacking of precipitates belonging to the same family as a result of annealing under stress along the indicated $[111]_{B2}$ direction. (Cao 2010; Cao 2011)

Moreover, when a material is annealed under stress, the Ni_4Ti_3 precipitates grow on **preferential** 111_{B2} planes so that ultimately only one family of precipitates will survive. In a single crystal sample of $Ni_{51}Ti_{49}$ annealed under $<111>_{B2}$ stress (10h, 550°C, 50MPa), the 3D investigation revealed box-like stackings of parallel precipitates as seen in Figure 4c (Cao 2010). As a result, the martensite plates are strongly directed in between these parallel precipitates, although no long pathways exist, again affecting the macroscopic behaviour (Michutta 2006). A similar phenomenon occurs in porous $Ni_{50.8}Ti_{49.2}$ material, aged for 6h at 500°C, where the stress field surrounding micron-sized pores can induce directional preference in the growth of the Ni_4Ti_3 precipitates, as seen in Figure 5 (Yao 2015).

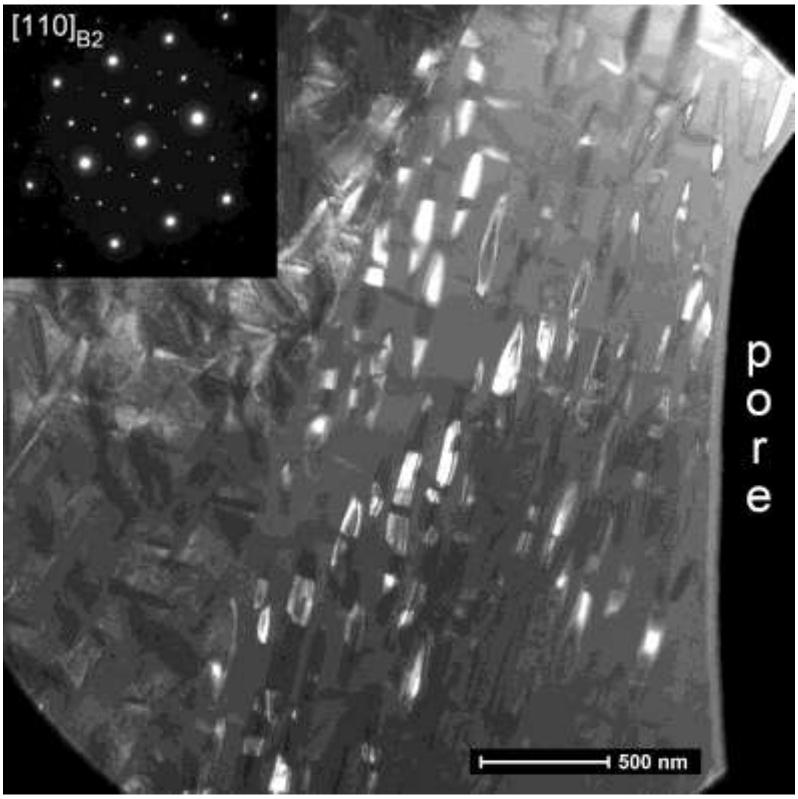

Figure 5: Ni_4Ti_3 precipitates grown next to a pore in annealed porous $Ni_{50.8}Ti_{49.2}$. In the grain at the edge of the pore, the precipitates are aligned and belong nearly all to the same family, as also seen from the diffraction inset, while in the next grain (left side) precipitates of all variants have comparable sizes.

Ni-Ti-X ternary systems

When binary Ni-Ti is alloyed with a third element, particular combinations of precipitates can occur depending on the solubility of the third element. For example, $\mathbf{Ni_{30}Ti_{50}Pd_{20}}$ is investigated in the search for materials with low hysteresis and where the systematic replacement of Ni by Pd gradually changes the lattice parameters of the austenite and martensite so as to reach the $\lambda_2 = 1$ condition needed for minimal hysteresis (Cui 2006). In this system several precipitation zones with different variants of tetragonal (C_{11b}) $Ti_2Pd(Ni)$ platelets in the austenite B2 matrix surrounding a single ellipsoid $Ti_2Ni(Pd)$ particle exhibiting a cubic (Fd3m) structure were observed (Figure 6) (Delville 2010). Outside of this precipitation zone the material is in its martensite B19 phase. It is assumed that during the annealing at 800°C for 5.5h and the following quench to room temperature local fluctuations of the B2 matrix composition lead to the precipitation of $Ti_2Ni(Pd)$ particles accompanied by a precipitation of $Ti_2Pd(Ni)$ platelets in their immediate surroundings. Upon cooling the B2 phase is retained in the immediate surroundings of the central $Ti_2Ni(Pd)$ precipitate since Ms is locally lowered due to a Pd depletion and/or a strengthening of the matrix by the coherent $Ti_2Pd(Ni)$ precipitates. Obviously, such local fluctuations and precipitation not only influence the local transformation but also hamper the search for the delicate balance between composition and lattice parameters.

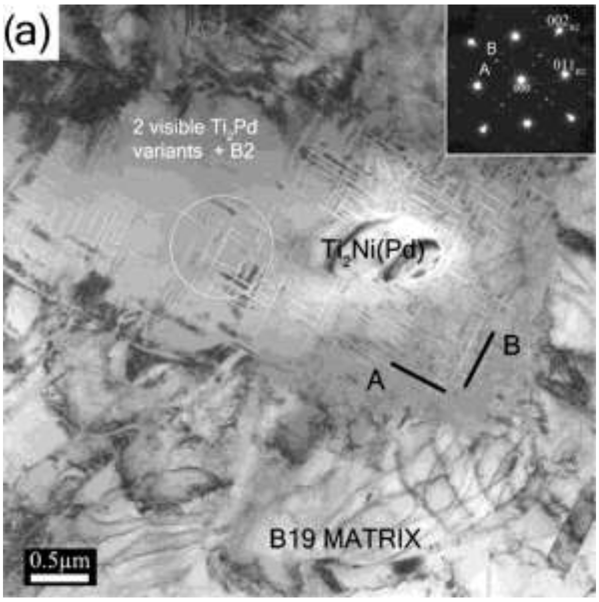

Figure 6: Complex precipitation zone with different crystallographic variants of platelet Ti_2Pd precipitates surrounding an ellipsoid $Ti_2Ni(Pd)$ particle in homogenized $Ni_{30}Ti_{50}Pd_{20}$. (Delville 2010)

On the other hand, in the **Ni-Ti-Nb** system the third element is added to increase the hysteresis. In this case, the Nb has very low solubility in the Ni-Ti matrix and a eutectic structure with Nb-rich particles is formed. Still, some Nb is retained in the matrix and depending on the cooling or annealing conditions this Nb further precipitates into nanoparticles. Although there is a large lattice misfit of 10% between the Nb-rich precipitates and the Ni-Ti matrix, both bcc based structures, there is a one-to-one correlation between the respective lattice orientations with the lattice misfit being accommodated by interface dislocations every 10/11 {110} lattice planes of the precipitate and matrix, resp., as seen in Figure 7a. This accommodation is very efficient so that only very little remaining strain inside the B2 matrix is observed. Although several investigations indicate that the response of the soft Nb-rich eutectic has the most pronounced effect on the transformation characteristics (Wang 2012; Zhao 1990), also these smaller precipitates can play an important role. Not only do they reduce the Nb content of the matrix, thus affecting the transformation temperatures via the concentration dependence (Shi 2014), but they also hamper the movement of the transformation front as seen in the captured image of an in-situ TEM annealing sequence where the austenite-martensite interface is seen to be halted by rows of precipitates formed in a commercial $(Ni\text{-}Ti)Nb_{8.4}$ alloy extruded and quenched from 900°C (Figure 7b) (Shi 2012). The latter already nucleate as aligned nanoscale precipitates along cubic directions of the austenite matrix in homogenized and quenched samples as seen in Figure 7c.

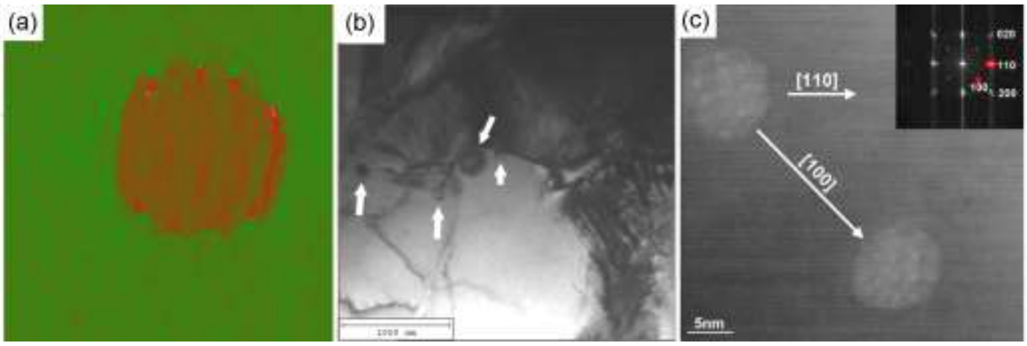

Figure 7: (a) GPA of Nb-rich nanosized precipitate in Ni-Ti-Nb revealing equidistant interface dislocations (as hotspots) accommodating the 10% lattice mismatch between precipitate and matrix. (b) Austenite-martensite interface blocked by rows of nanosized precipitates. (c) Two nano-precipitates aligned along a cubic austenite direction. (Shi 2012; Shi 2014)

Conclusions

In conclusion it can be stated that the formation of secondary phases by short or long-range diffusion, often as nano-sized precipitates, can have a profound effect on the shape memory and superelastic potential of a material undergoing a martensitic transformation. Depending on the case at hand, such secondary phases can decrease the probability of a displacive transformation by changing the phase stability in the system or can mechanically hinder the passage of the transformation interface. On the other hand, properly controlling the nucleation and growth of some precipitates can strongly improve the properties of some types of materials.

Acknowledgments

The author gratefully thanks all researchers involved in the S/TEM investigations of the above listed examples: Y. Ma (NiAl), W. Tirry, Z.Q. Yang, S. Cao (NiTi), R. Delville (NiTiPd), H. Shi, (NiTiNb). The Flemish Science Foundation as well as the European Commission are acknowledged for financial support on various projects.

References

Bataillard L, Bidaux J-E, Gotthardt R (1998) Interaction between microstructure and multiple-step transformation in binary NiTi alloys using in-situ transmission electron microscopy observations. Philosophical Magazine A 78:327-344

Bradley AJ, Taylor A (1937) An X-ray analysis of the nickel–aluminium system. Proc. R. Soc. Lond. A 159:56-72

Cao S, Somsen C, Croitoru M, Schryvers D, Eggeler G (2010) Focused ion beam/scanning electron microscopy tomography and conventional transmission electron microscopy assessment of Ni_4Ti_3 morphology in compression-aged Ni-rich Ni-Ti single crystals. Scripta Materialia 62:399-402

Cao S, Nishida M, Schryvers D (2011) Quantitative three-dimensional analysis of Ni_4Ti_3 precipitate morphology and distribution in polycrystalline Ni-Ti. Acta Materialia 59:1780-1789

Cao S, Pourbabak S, Schryvers D (2012) Quantitative 3-D morphologic and distributional study of Ni_4Ti_3 precipitates in a $Ni_{51}Ti_{49}$ single crystal alloy. Scripta Materialia 66:650-653

Cohen M, Olson GD, Clapp PC (1979) On the classification of displacive phase transformations; Proceedings of international conference on martensitic transformations. Proceedings of International Conference on Martensitic Transformations ICOMAT-79:1-6

Cui J, Chu YS, Famodu OO, Furuya Y, Hattrick-Simpers J, James RD et al. (2006) Combinatorial search of thermoelastic shape-memory alloys with extremely small hysteresis width. Nature Materials, 5:286-290

Delville R, Schryvers D (2010) Transmission electron microscopy study of combined precipitation of $Ti_2Ni(Pd)$ and $Ti_2Pd(Ni)$ in a $Ti_{50}Ni_{30}Pd_{20}$ alloy. Intermetallics 18:2353-2360

Dlouhy A, Khalil-Allafi J, Eggeler G (2003) Multiple-step martensitic transformations in Ni-rich NiTi alloys—an in-situ transmission electron microscopy investigation. Phil. Mag. 83:339-363.

Frenzel J, George EP, Dlouhy A, Somsen C, Wagner M-X, Eggeler G (2010) Influence of Ni on martensitic phase transformations in niti shape memory alloys. Acta Materialia 58:3444-3458

Hÿtch MJ, Snoeck E, Kilaas R (1998) Quantitative measurement of displacement and strain fields from HREM micrographs. Ultramicroscopy 74:131-146

Jansen J, Tang D, Zandbergen HW, Schenk H (1998) MSLS, a least-squares procedure for accurate crystal structure refinement from dynamical electron diffraction patterns. Acta Crystallographica Section A: Foundations of Crystallography 54:91-101

Jansen J, Zandbergen HW (2002) Determination of absolute configurations of crystal structures using electron diffraction patterns by means of least-squares refinement. Ultramicroscopy 90:291-300

Khalil-Allafi J, Dlouhy J, Eggeler G (2002) Ni_4Ti_3-precipitation during aging of NiTi shape memory alloys and its influence on martensitic phase transformations Acta Materialia 50:4255-4274

Khalil-Allafi J, Ren X, Eggeler G (2002) The mechanism of multistage martensitic transformations in aged Ni-rich NiTi shape memory alloys. Acta Materialia 50:793-803

Michutta J, Somsen C, Yawny A, Dlouhy A, Eggeler G (2006) Elementary martensitic transformation processes in Ni-rich NiTi single crystals with Ni_4Ti_3 precipitates. Acta Materialia 54:3525-3542

Nishida M, Hara T, Ohba T, Yamaguchi K, Tanaka K, Yamauchi K (2003) Experimental consideration of multistage martensitic transformation and precipitation behavior in aged Ni-rich Ti-Ni shape memory alloys. Materials Transactions 44:2631-2636

Okamoto H (2004) Al-Ni (Aluminum-Nickel). Journal of Phase Equilibria and Diffusion 25:394

Otsuka K, Ren X (2005) Physical metallurgy of Ti-Ni-based shape memory alloys. Progress in Materials Science 50:511-678

Schryvers D (1993) Microtwin sequences in thermoelastic Ni_xAl_{100-x} martensite studied by conventional and high-resolution transmission electron microscopy. Philosophical Magazine A 68:1017-1032

Schryvers D, Ma Y, Toth L, Tanner L (1995) Electron microscopy study of the formation of Ni_5Al_3 in a $Ni_{62.5}Al_{37.5}$ B2 alloy I. Precipitation and growth. Acta Metallurgica et Materialia 43:4045-4056

Schryvers D, Ma Y, Toth L, Tanner L (1995) Electron microscopy study of the formation of Ni_5Al_3 in a $Ni_{62.5}Al_{37.5}$ B2 alloy II. Plate crystallography. Acta Metallurgica et Materialia 43:4057-4065

Schryvers D, Ma Y (1995) In situ TEM study of the Ni_5Al_3 to B2+$L1_2$ decomposition in $Ni_{65}Al_{35}$. Materials Letters 23:105-111

Shapiro SM, Yang BX, Noda Y, Tanner LE, Schryvers D (1991) Neutron-scattering and electron-microscopy studies of the premartensitic phenomena in Ni_xAl_{100-x} alloys. Phys Rev B Condens Matter 44:9301-9313

Shi H, Pourbabak S, Van Humbeeck J, Schryvers D (2012) Electron microscopy study of Nb-rich nanoprecipitates in Ni-Ti-Nb and their influence on the martensitic transformation. Scripta Materialia 67:939-942

Shi H, Frenzel J, Martinez GT, Van Rompaey S, Bakulin A, Kulkova S et al (2014) Site occupation of nb atoms in ternary Ni-Ti-Nb shape memory alloys. Acta Materialia 74:85-95

Tang W (1997) Thermodynamic study of the low-temperature phase B19 and the martensitic transformation in near-equiatomic Ti-Ni shape memory alloys. Metallurgical and Materials Transactions A 28:537-544

Tirry W, Schryvers D (2005) Quantitative determination of strain fields around Ni_4Ti_3 precipitates in NiTi. Acta Materialia 53:1041-1049

Tirry W, Schryvers D, Jorissen K, Lamoen D (2006) Electron-diffraction structure refinement of Ni_4Ti_3 precipitates in $Ni_{52}Ti_{48}$. Acta Crystallographica B 62:966-971

Tirry W, Schryvers D (2009) Linking a completely three-dimensional nanostrain to a structural transformation eigenstrain. Nature Materials 8:752-757

Wang M, Jiang M, Liao G, Guo S, Zhao X (2012) Martensitic transformation involved mechanical behaviors and wide hysteresis of NiTiNb shape memory alloys. Progress in Natural Science: Materials International 22:130-138

Wang X, Kustov S, Li K, Schryvers D, Verlinden B, Van Humbeeck J (2015) Effect of nanoprecipitates on the transformation behavior and functional properties of a Ti-50.8 at.% Ni alloy with micron-sized grains. Acta Materialia 82:224-233

Yang Z, Tirry W, Schryvers D (2005) Analytical TEM investigations on concentration gradients surrounding Ni_4Ti_3 precipitates in Ni-Ti shape memory material. Scripta Materialia 52:1129-1134

Yang Z, Tirry W, Lamoen D, Kulkova S, Schryvers D (2008) Electron energy-loss spectroscopy and first-principles calculation studies on a Ni-Ti shape memory alloy. Acta Materialia 56:395-404

Yao X, Cao S, Zhang XP, Schryvers D (2015) Microstructural characterization and transformation behavior of porous $Ni_{50.8}Ti_{49.2}$. Materials Today, Proceedings of International Conference on Martensitic Transformations ICOMAT-2014 (to be published)

Zhao LC, Duerig TW, Justi S, Melton KN, Proft JL, Yu W, Wayman CM (1990) The study of Niobium-rich precipitates in a Ni-Ti-Nb shape memory alloy. Scripta Metallurgica et Materialia 24:221-225